

# ENGINEERING DAMAGE INDICATORS BASED ON ADVANCED FINITE ELEMENT MODELLING

**F. DUFOUR\***, **C. GIRY<sup>†</sup>**, **J. MAZARS\*** AND **M. SOUFFLET<sup>†</sup>**

\*Grenoble-INP / University Joseph Fourier / CNRS UMR 5521  
3SR laboratory, BP 53, Grenoble, France  
e-mail: frederic.dufour@3sr.grenoble-inp.fr, web page: www.3s-r.hmg.inpg.fr

<sup>†</sup>LMT Cachan/Univ.Paris 6/CNRS/PRES UniverSud.  
61, Avenue du Prsident Wilson, 94230 Cachan, France  
e-mail: Cedric.Giry@ens-cachan.fr, web page: www.lmt.ens-cachan.fr

**Key words:** Crack properties, damage, nonlocal method, reinforced concrete

**Abstract.** In engineering practice, the durability of concrete structures is usually, as in European standard (EC2) dealt with crack opening and spacing in order to limit the corrosion risk for rebars due to the penetration of chemical agents coming from the environment of the structure.

The advanced numerical modelling of cracking in reinforced concrete structures may be dealt with either by means of discontinuous models (fracture mechanics, X-FEM, G-FEM, etc.) or using continuous constitutive models such as damage mechanics. The issue of this contribution is to propose a procedure to get crack path and its opening along the path.

The method is based on a topological search of the crack path following the ridge formed by the equivalent strain field in a 2D plane. 3D crack surfaces can be assessed by slicing the computational domain in 2D planes. Along this surface, at discrete points the crack opening equivalent to the strong discontinuity approach can be computed. This procedure has already been applied in a 2D context and validated against experimental results obtained by digital image correlation for a 3 point bending beam.

More recently, the representation of the strain field has been largely improved by introducing the effect of the stress field into the space averaging procedure of the nonlocal integral approach. The consequence is a more accurate estimation of the crack opening since the strain field is closer to the one obtained by discrete approach, in contrary to the original version of the nonlocal approach.

The complete procedure is applied to a full size reinforced concrete beam submitted to a four point bending test. The influence of the rebar diameter and the concrete cover are analysed on the crack pattern and the crack opening.

## 1 INTRODUCTION

In engineering practice, the durability of concrete structures is usually, as in European standard (EC2) dealt with crack opening and spacing in order to limit the corrosion risk for rebars due to the penetration of chemical agents coming from the environment of the structure.

The bottleneck is to estimate as accurately as possible crack path (from which crack spacing is deduced) and crack opening for any material properties and structural geometries.

This goal can be partially assessed by means of discontinuous models (fracture mechanics, X-FEM, G-FEM, etc.) for which the crack opening is part of the constitutive law. However,

since those models deal with crack propagation criteria, crack initiation is not properly determined and a lot of effort (mesh size) must be put in the computational scheme to get objective paths.

Since regularized damage mechanics have been successfully used to model concrete structure behaviour from initiation to complete failure, the authors have developed a strategy to compute in post-treatment procedures the main crack properties (path and opening) for engineering applications.

In the first part, a recent improvement of the non-local regularization technique is recalled, then the two consecutive procedures to compute the crack path and opening. In the last part of this contribution, the complete method is applied to a concrete structures in 3D.

## 2 CHARACTERIZATION OF STRAIN LOCALIZATION AND DAMAGE IN QUASI-BRITTLE MATERIAL

### 2.1 Continuous damage model

The degradation of concrete is described, in this contribution, by means of an isotropic damage model to represent the progressive loss of stiffness at the scale of the fracture process zone.

The model introduces a scalar damage variable  $D$  that links the Cauchy stress tensor  $\boldsymbol{\sigma}$  and the strain tensor  $\boldsymbol{\varepsilon}$  (eq. 1) :

$$\boldsymbol{\sigma} = (1 - D)\mathbf{C} : \boldsymbol{\varepsilon} \quad (1)$$

with  $\mathbf{C}$ , the fourth order elastic tensor.

This damage variable  $D$  is driven by a state variable  $Y$  expressed as the largest value ever reached of  $\varepsilon_{eq}$  defined by Mazars [1] (eq.2):

$$\varepsilon_{eq} = \sqrt{\sum_{i=1}^3 \langle \varepsilon_i \rangle_+^2} \quad (2)$$

with  $\varepsilon_i$  the principal strains.  $\langle \cdot \rangle_+$  defines the Mac Cauley brackets. The time evolution over the loading history of  $Y$  respects the Kuhn-Tucker conditions (eq. 3) and is equal to the strain damage threshold  $\varepsilon_{D_0}$  initially.

$$\varepsilon_{eq} - Y \leq 0, \quad \dot{Y} \leq 0, \quad \dot{Y} \cdot (\varepsilon_{eq} - Y) = 0 \quad (3)$$

Several damage evolution laws do exist, in this contribution the following one has been used:

$$D_{t,c} = 1 - \frac{\varepsilon_{D_0}(1 - A_{t,c})}{Y} - \frac{A_{t,c}}{e^{[B_{t,c}(\bar{Y} - \varepsilon_{D_0})]}} \quad (4)$$

where  $A_t$ ,  $A_c$ ,  $B_t$  and  $B_c$  are four parameters of the model.  $D_t$  and  $D_c$  are damage in traction and compression respectively. The damage variable  $D$  is a linear combination of these two variables such as:

$$D = \alpha_t D_t + \alpha_c D_c \quad (5)$$

where  $\alpha_t$  and  $\alpha_c$  characterize the traction and the compression part of the loading respectively.

### 2.2 Stress-based nonlocal damage model

It is now well known that models used to describe the failure of quasibrittle materials, by introducing a softening behavior, necessitate the addition of a regularization method in order to maintain the objectivity of the results with respect to the space discretisation.

Numerous regularization models have been proposed in the past; among them, the strain gradient enhanced media [2] or the nonlocal model [3] are widely used for concrete structure analysis. The reader can find a large review of these models in [4]. The nonlocal model proposed by Pijaudier-Cabot and Bažant in [3] replaces the local equivalent strain  $\varepsilon_{eq}$  by its nonlocal counterpart  $\bar{\varepsilon}_{eq}$  (eq. 6).

$$\bar{\varepsilon}_{eq}(\mathbf{x}) = \frac{\int_{\Omega} \phi(\mathbf{x} - \mathbf{s}) \varepsilon_{eq}(\mathbf{s}) d\mathbf{s}}{\int_{\Omega} \phi(\mathbf{x} - \mathbf{s}) d\mathbf{s}} \quad (6)$$

with  $\phi(\mathbf{x} - \mathbf{s})$  a weighting function. The Gaussian function has been chosen in the present study (eq.7).

$$\phi(\mathbf{x} - \mathbf{s}) = \exp\left(-\left(\frac{2\|\mathbf{x} - \mathbf{s}\|}{l_c}\right)^2\right) \quad (7)$$

with  $l_c$  the internal length of the model and  $\|\mathbf{x} - \mathbf{s}\|$  the distance between points at  $\mathbf{x}$  and  $\mathbf{s}$  locations.

This model has shown its efficiency as a regularization method by keeping unchanged the

mechanical response upon finite mesh refinement. It is also capable to reproduce accurately the material size effect. Nevertheless, it fails to describe both the strain localization close to failure leading to an unwilling diffusion of damage at the location of the fracture process zone and damage initiation close to boundaries.

In the framework of nonlocal integral models, several propositions have been made in the last decade to address those problems. For instance, one can quote the works of Pijaudier-Cabot and coworkers in [5] to deal with boundary effects and of Pijaudier-Cabot and Dufour in [6] and of Desmorat and Gatuingt in ([7]) that manage to improve the strain localization description but at an expensive computational time cost. However, since an open crack can be regarded as a newly formed boundary, a unified approach should be capable to account for both boundaries and strain localization at a crack location. More recently, the authors have proposed in [8] a modification of the original nonlocal integral model by introducing the influence of the stress state on the nonlocal interactions between neighboring points (Eq.8) by means of a scalar coefficient  $0 \leq \rho \leq 1$  that multiplies the internal length.

$$\phi(\mathbf{x} - \mathbf{s}) = \exp \left( - \left( \frac{2 \|\mathbf{x} - \mathbf{s}\|}{l_c \rho(\mathbf{x}, \boldsymbol{\sigma}_{prin}(\mathbf{s}))} \right)^2 \right) \quad (8)$$

with  $\rho$  depending on the principal stress tensor  $\boldsymbol{\sigma}_{prin}(\mathbf{s})$  at  $\mathbf{s}$  (10).

$$\rho(\mathbf{x}, \boldsymbol{\sigma}_{prin}(\mathbf{s}))^2 = \frac{1}{f_t^2 \left( \frac{\sin^2 \varphi \cos^2 \theta}{\sigma_1^2(\mathbf{s})} + \frac{\sin^2 \varphi \sin^2 \theta}{\sigma_2^2(\mathbf{s})} + \frac{\cos^2 \varphi}{\sigma_3^2(\mathbf{s})} \right)} \quad (9)$$

with  $f_t$  the tensile strength of the material,  $\sigma_1(\mathbf{s})$ ,  $\sigma_2(\mathbf{s})$  and  $\sigma_3(\mathbf{s})$  the principal stresses and  $\mathbf{u}_1(\mathbf{s})$ ,  $\mathbf{u}_2(\mathbf{s})$ , and  $\mathbf{u}_3(\mathbf{s})$  the vectors associated to the principal directions.  $\theta$  is the angle between  $u_1$  and the projection of  $(\mathbf{x} - \mathbf{s})$  onto the plane defined by  $u_1$  and  $u_2$ , and  $\varphi$  is the angle between  $u_3$  and  $(\mathbf{x} - \mathbf{s})$ . Giry and coworkers have shown that this model improves the description of both the nonlocal quantities close to boundaries and the strain localization at complete failure compared to the original model.

Moreover it has the advantage to avoid additional computational time and does not introduce new parameter always difficult to calibrate from experiments.

### 3 FROM CONTINUOUS MODELLING TO DISCRETE INFORMATION

The continuous approach presented previously allows to describe the degradation of a structure under severe loadings up to failure. The cracking observed in the structure is quantified cinematically in terms of a continuous strain field. In order to obtain engineering damage indicators as crack opening or spacing, an additional step is needed to convert continuous results into discrete information.

#### 3.1 Quantification of crack opening

The method considers in this study to quantify the crack opening is the one developed by Dufour and coworkers in [9]. The main idea is the comparison of the continuous strain field obtained by the calculation and an analytical strain field corresponding to a strong discontinuity displacement field (Fig.1). The main steps of the method are recall here.

To estimate crack opening at a point of the crack, the strain field obtained from the calculation is projected along a line perpendicular to the crack (see 3.2 for crack path). As a comparison versus a Dirac like function (strain profile of the strong discontinuity, Fig.2) cannot be performed mathematically, a convolution product with a Gaussian function is applied to both profiles (Fig.3).

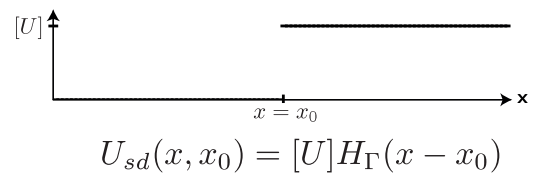


**Figure 1:** Displacement profile of a strong discontinuity.

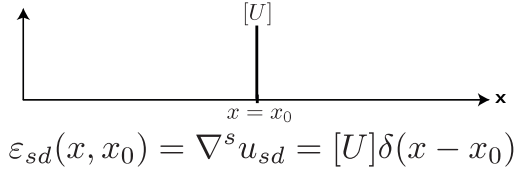


Figure 2: Strain profile of a strong discontinuity.

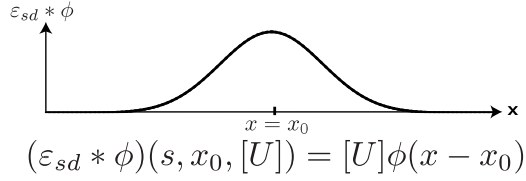


Figure 3: Convolution product of a profile of a strong discontinuity with a Gaussian function.

Under the hypothesis of an equal intensity of both convoluted products at the crack location, an estimation of crack opening is obtained (Eq.10).

$$[U] = \frac{(\varepsilon_{FE} * \phi)(x_0) \int_{\ell} \phi(x_0 - x) dx}{\phi(0)} \quad (10)$$

with  $\varepsilon_{FE}$  the finite element strain field along the 1D profile  $\ell$ .  $*$  corresponds to the convolution product and  $\phi$  has been chosen as the Gaussian function for the analysis.  $x_0$  is the coordinate along the 1D profile of the crack location.

On top of the crack opening this method also provides an estimator of the error made by comparing the finite element strain profile with a strong discontinuity one. This procedure has already been applied in a 2D context and validated against experimental results obtained by digital image correlation for a 3 point bending beam.

### 3.2 Location of the crack path

A preliminary step for the quantification of crack opening is the determination of the crack location from a continuous field. Different methods have been developed to deal with this problem. One can quote the method proposed by Dufour and coworkers in [10] who consider an equivalent thermal analysis with the direction associated to the maximum principal strain identified as the direction of the heat flow. The

compatible crack paths correspond to isothermals perpendicular to the direction of the heat flow, i.e. maximum principal strain. At the end, the isothermal corresponding to the crack path is the one passing through the Gaussian point with the highest nonlocal equivalent strain (Eq.6).

Other techniques have been developed by considering a geometrical approach of the problem. Tamayo and Rodriguez-Ferran in [11] identify the crack path as the line formed by circle centers included in the damaged band representing the fracture process zone. The method considered in this study is the one proposed by Bottoni and Dufour in [12] to identify the crack path from a 2D continuous analysis for which a step-by-step procedure is proposed to follow the ridge of a field characterizing the degradation of the structure. The internal variable field has been found to be the most robust since its value is not limited to 1 as compared to the damage field. Thus, the ridge is steeper.

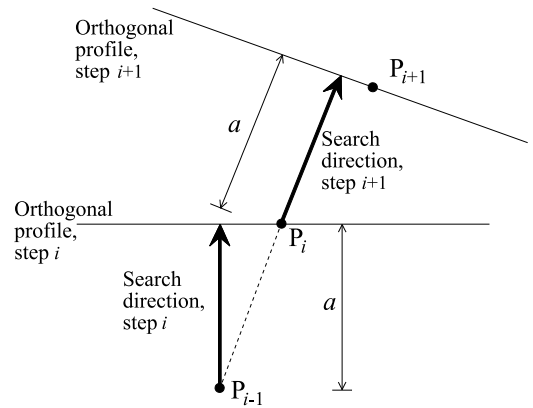
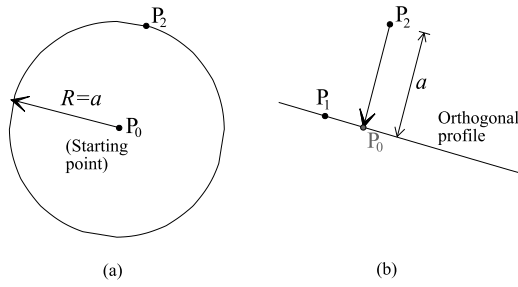


Figure 4: Illustration of the process considered to identify a point of the crack.

The current step needs the definition of a starting point and of a search direction, which are respectively the point  $P_i$  found in the previous step and the direction  $\overrightarrow{P_{i-1}P_i}$  determined by the last two points found. Following operations are performed, see the scheme in Fig. (4):

1. a prediction point  $s_0$  is defined by moving from the previously found point  $P_{i-1}$  in the search direction, at a distance  $a$  called “search length”;

2. the field  $Y(x, y)$  is projected onto a line of length  $l_{orth}$ , perpendicular to the search direction, obtaining the function  $Y(s)$ ;  $s$  being the abscissa on this line with origin  $s_0$
3. the function  $Y(s)$  is smoothed out to obtain the new function  $\bar{Y}(s)$  by means of a convolution product, given by equation (6) with  $l_{smooth}$  as the internal length. The new ridge point  $P_{i+1}$  is the point where  $\bar{Y}(s)$  is maximum.



**Figure 5:** Initialisation of the topological search.

Since no search direction is provided initially, a specific procedure must be used. An approximation of the first point position (called  $P_0$ ) is where the field  $Y$  has its absolute maximum on the considered damaged zone; moreover, the orthogonal line of the current step can be replaced by a circle. More into details, following operations are executed (see also the scheme in Fig. 5):

1. the field  $Y(x, y)$  is projected onto a circle, having center in  $P_0$  and radius equal to the search length  $a$ , so to obtain the field  $Y(s)$  (Fig. 5a);
2. the projected field  $Y(s)$  is smoothed by applying equation (6) on the circle with  $l_{smooth}$  as the internal length, the second ridge point  $P_2$  is the point where the smoothed field  $\bar{Y}(s)$  is maximum (Fig. 5a); unlike  $P_0$ ,  $P_2$  is obtained from the smoothed field, so it belongs to the crack path;

3. a back-correction is made to find the real position for the first point  $P_1$ , by projecting and smoothing the field on the line through  $P_0$  and orthogonal to  $\overrightarrow{P_2P_0}$  (Fig. 5b); this correction is necessary because without the smoothing, the first point position would be too sensitive to the mesh;
4. two possible search directions are determined by the points  $P_1$  and  $P_2$ , i.e.  $\overrightarrow{P_1P_2}$  and  $\overrightarrow{P_2P_1}$ ; the search continues in one of the identified directions as previously detailed until stop requirements are fulfilled (i.e. the maximum value of  $\bar{Y}$  is below a predefined value corresponding to the damage threshold for instance) then it is pursued in the second direction. Doing so, the procedure is applicable for both cases when the initial point is an end point of the crack (crack mouth) or a middle point.

Fig. 6 illustrates the application of this procedure to a traction test with an inclusion. The crack path perfectly follows the ridge of the damage field, i.e. the crack follows the central part of the fracture process zone.

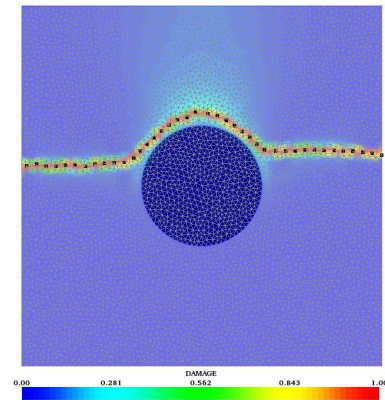


**Figure 6:** Traction test with an inclusion. Damage field and crack path (black squares).

### 3.3 From 2D to 3D analysis

The method introduced previously to determine the crack path has been developed for 2D analysis since there is no ridge definition for a

3D field. As a consequence, an additional effort has to be made for the post-treatment of a 3D field. In order to keep the 2D post-treatment method, a simple slicing procedure is considered with a projection of the fields used for the post-treatment (internal variable and equivalent strain) onto the slicing plans.



Figure 7: Example of definition of slicing plans.

A peculiar attention should be paid to the orientation of the slicing plans in order to get an estimation as accurate as possible for the crack opening. More particularly, this plan should include the direction of the maximum principal strain as it corresponds to the direction of crack opening for mode I failure. An average direction is computed from the maximum principal strain directions extracted among the elements that observe a damage initiation (Fig. 7).

#### 4 ANALYSIS OF A REINFORCED CONCRETE BEAM UNDER 4 POINTS BENDING

The study presented here is a part of a French national project (CEOS.fr) whose scope is the analysis and the identification of the material and geometrical parameters influence on cracking in reinforced concrete structural elements. The results shown hereafter are an extract of the whole numerical campaign performed. The main objective here is to analyse the capability of the constitutive nonlocal model and the different approaches presented in the previous parts to characterize the behavior of a rein-

forced concrete structure at a global scale and to extract local quantities.

#### 4.1 Presentation of the study

The analysis is performed on a reinforced concrete beam under 4 point bending loading. The specimen dimensions are 5.1 m of span, 0.8 m of height and 0.47 m of depth. Fig.8 gives the reinforced concrete cross section of the beam. Three longitudinal rebars are placed in the lower part and in the upper part with a diameter  $\phi_1$  and  $\phi_2$  respectively. A concrete cover of  $c_2$  is introduced at the top and the bottom of the beam.

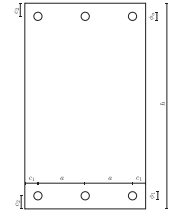


Figure 8: Representation of the 4 point bending test and the reinforced concrete section associated.

Tab.1 summarizes the geometrical characteristics for the three different tests considered.

Table 1: Geometrical parameters for the test

	TEST A	TEST B	TEST C
$c_2$ (mm)	51	66	86
$\phi_1$ (mm)	32	32	32
$\phi_2$ (mm)	25	25	25

The same concrete is casted in this study corresponding to a "C56" concrete with the following characteristics using EC2 notations:  $f_{c_m} = 64$  MPa,  $f_{c_k} = 56$  MPa,  $f_{t_m} = 4.4$  MPa and  $E_{c_m} = 40.8$  GPa. The characteristics of the steel rebars are the following ones:  $f_{y_k} = 500$  MPa and  $E_{y_k} = 210$  GPa. In order to reproduce the nonlinear behavior of the concrete, the following model parameter are identified:  $E_c = 40.8$  GPa,  $\nu = 0.18$ ,  $\varepsilon_{D_0} = 10^{-4}$ ,  $A_t = 0.9$ ,  $B_t = 6000$ ,  $A_c = 1.8$ ,  $B_c = 1400$  and  $l_c = 45$  mm. As the objective of the study is to analyse mode I cracking, this nonlinear model is used only in

the central part of the beam (area of constant bending moment) and outside, a linear elastic behavior is considered. Furthermore, it allows to avoid damage initiation in the neighborhood of loading area. An area of transition is introduced between the linear and the nonlinear parts with a threshold for damage initiation taken sufficiently high. It allows to give a complete domain of integration for the regularization procedure. Indeed, Pijaudier-Cabot and coworkers have shown in [5] that a truncated domain of integration domain for nonlocal integral method leads to an attraction of damage close to boundary. For the symmetry planes, classical conditions are considered regarding nonlocal integral regularization method with the introduction of a complementary domain to compute the nonlocal integral values. As serviceable loadings are considered in this study, a linear elastic model is used for steel reinforcement:  $E_s = 210$  GPa and  $\nu = 0.2$ .

Due to symmetry, only a quarter of the beam is considered for the study. Although it imposes a symmetry for the cracking mode, the reduction of computational time obtained is put forward. Fig.8 gives a representation of the mechanical problem analysed with the vertical imposed displacement  $\delta$  up to 0.01 m.

A volumetric mesh is used to describe the geometry of the specimen. The lower reinforcements are explicitly defined through cubic and prismatic elements with linear interpolation functions. This level of precision is necessary has the influence of the concrete cover and the diameter of the rebars is observed. In contrary, for the upper reinforcements, a lower precision is required and bar elements with linear interpolation functions are considered. Two different mean mesh sizes are used to describe the whole beam, a fine mesh for the central part ( $d_{fine} = 0.015$  m) and a coarse mesh for the other parts ( $d_{coarse} = 0.06$  m).

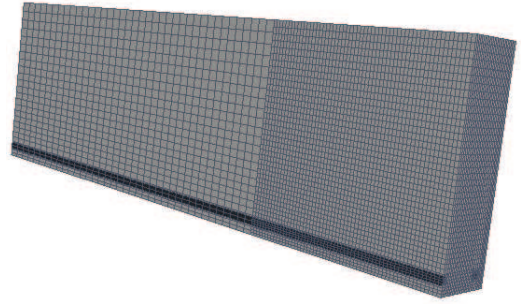


Figure 9: Example of a mesh used for the study (TEST A).

## 4.2 Analysis of the results

Fig.10 shows the global behavior observed for the different beams.

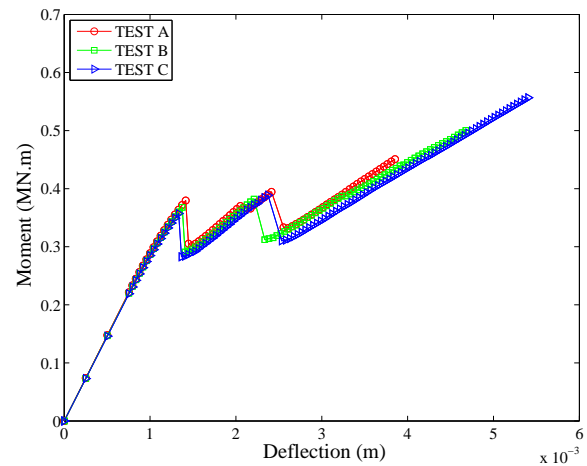


Figure 10: Bending moment in the central part versus deflection.

One can observe a similar global behavior between the different tests. Only small discrepancies appear for the load levels at cracks initiations. Asymptotically, as we could expect, the small variation of the concrete cover between beams does not affect significantly the behavior with the highest rigidity for the smallest concrete cover.

Fig.11 shows the cracking observed in the beam at two different loading levels. The location of the cracks is identified with the latest step considered for the post-treatment. The two cracks observed on Fig.11 are described thanks to three profiles corresponding to the three slicing planes used for the projection of the post-treated fields. The parameters of the topological

search method are:  $l_{orth} = 0.15$  m,  $a = 0.015$  m,  $l_{smooth} = 0.05$  m.

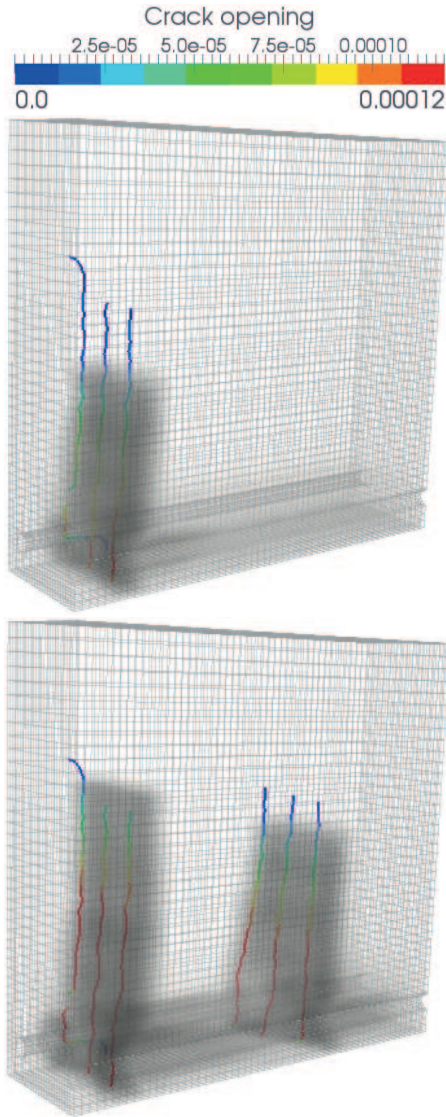


Figure 11: Examples of 3D damage field and the corresponding 3D cracks identified on three slicing plans (TEST B) for two applied deflections:  $\delta = 1.4$  mm and 2.2 mm.

The first crack initiates under the loading area due to the perturbation of the stress field with an higher value compared to the ones in the constant bending moment area. After a phase of crack propagation, a progressive degradation of the steel concrete bond is observed, characterized by a cylindrical damaged area around the lower reinforcements. At some distance, a second crack initiates as the stress redistributed by the reinforcement reaches the damage thresh-

old.

The development of the main cracks can also be followed thanks to information one can get from the stress state along the reinforcements. Fig.12 shows the evolution of  $\sigma_{xx}$  profile along a rebar during the loading.

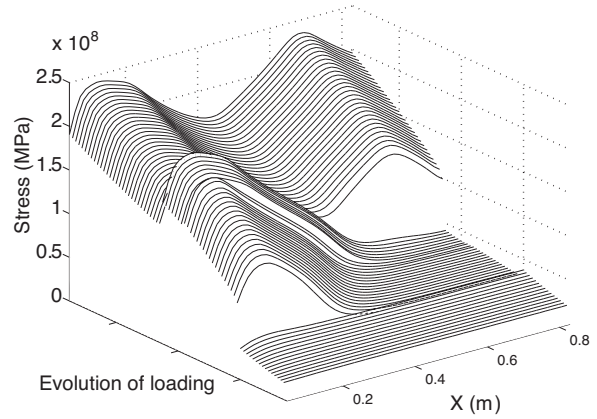


Figure 12: Evolution of the axial stress profile along a lower reinforcement during the loading (TEST A).

One can observe that the appearance of a new crack leads to a stress jump in the reinforcement at the location of the crack. As a new crack forms, a phenomenon of local unloading is observed for the steel close to previous cracks corresponding to the decrease of the global carried load.

Tab.2 summarizes the spacing between the two first main cracks for the different tests for an applied deflection of 3 mm.

**Table 2:** Spacing between the main cracks

	TEST A	TEST B	TEST C
crack spacing (m)	0.503	0.424	0.504

From these results, no real correlation can be identified between the concrete cover and the crack spacing. It should be quoted that in a second step during the loading, small cracks appear in the bottom of the structure before joining existing main cracks (Fig.13). These secondary cracks seem to appear preferentially for small concrete cover as one can see for Test A.

The distance between main cracks and this secondary cracks may evolve with the distance that can change with the concrete cover. Moreover, the crack spacing is perturbed in a real structure by the presence of stirrups playing the role of inclusions.

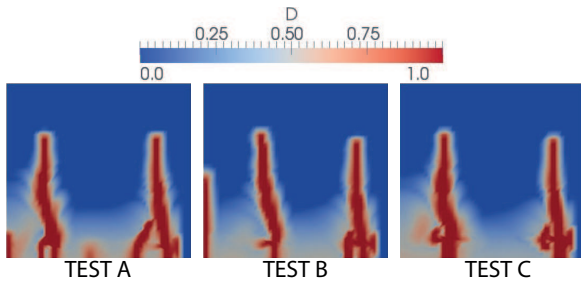


Figure 13: Illustration of the development of secondary cracks with the damage fields for the three test.

Regarding crack opening, Fig.14 gives the evolution of crack opening along the height of the beam. This evolution is considered for a profile crossing the cover and a profile between two rebars.

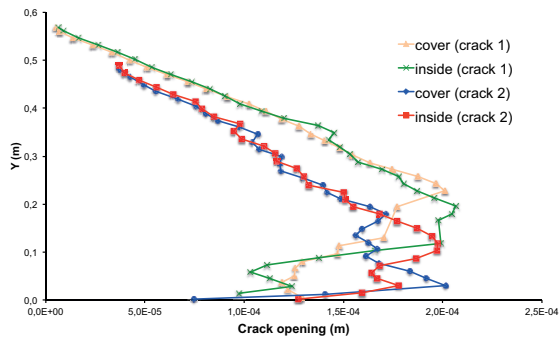


Figure 14: Evolution of the crack opening along the height of the beam for an imposed displacement  $\delta = 3$  mm (TEST A).

One can observe that the rebars act as crack opening limiters. Indeed, above a certain height, the evolution of the crack opening is linear whereas close to the location of the reinforcements, the crack opening tends to decrease. Fig.15 shows the influence of the concrete cover on the crack opening profile.

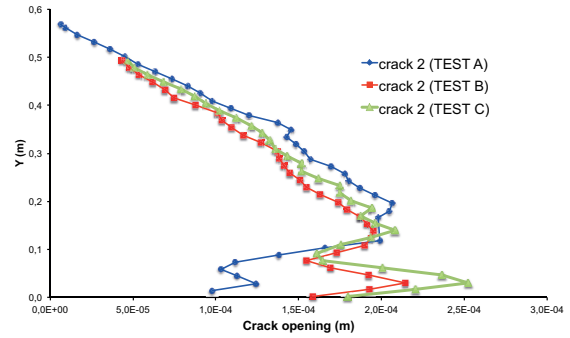


Figure 15: Crack opening along the height of the beam for an imposed displacement  $\delta = 3$  mm (TEST A, B and C).

The crack opening profile above the rebars are similar. In contrary, one can observe that under the rebars it tends to increase with the increase of the concrete cover. This is due to the fact that a high value for the concrete cover allows the development of the crack between the rebar and the outside surface of the beam.

Fig.16 gives the evolution during the loading of the crack opening profile for the first crack (test B).

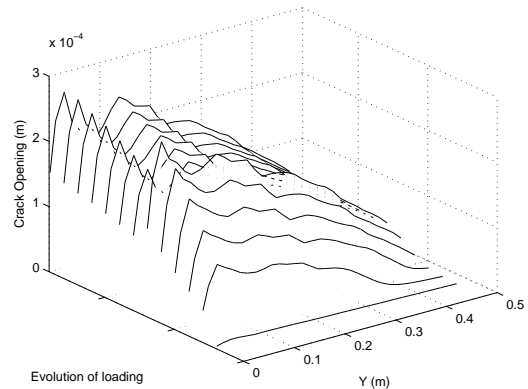


Figure 16: Evolution of the crack opening profile during the loading (TEST B).

One can observe that the degradation of the structure is relatively brittle with a fast development of the crack as soon as it has passed the reinforcements. After this first step, a regular evolution of the crack opening is observed along the crack profile. Then, as it has already been observed in Fig.12 a small unloading of

the crack is observed upon the propagation of a new crack.

## 5 CONCLUSIONS

This contribution shows that crack properties (spacing and opening) can be assessed by means of a continuous damage model. A damage model regularized by an innovative nonlocal approach taking advantage of the stress field is used to reproduce the progressive cracking process from initiation up to complete failure. In a post-treatment step, crack path and opening can be estimated at a reasonable computational cost. A step-by-step procedure has been developed to follow the ridge of the damaged zone and along this line a displacement jump (i.e., the crack opening) is computed by comparison with the strong discontinuity approach. The performance of these procedures are highlighted on four point bending tests with different covers to analyse its effect on crack opening values. This contribution demonstrates that engineering damage indicators can be estimated by advanced modelling. This is a step forward for predictive methods of concrete structure behaviour. The next perspective of this work is to add a third step that is the mass transfer properties in order to accurately assess structural tightness and/or durability.

## 6 ACKNOWLEDGEMENT

The investigations and results reported herein are supported by the French national program CEOS.fr sponsored by the ministry in charge of sustainable development (MEDDE) and the French National Research Agency (ANR) under the MEFISTO research program (control of cracking in concrete structures grant VD08\_323065).

## REFERENCES

- [1] Mazars J., 1986. A description of micro- and macroscale damage of concrete structures, *Eng. Frac. Mech.* **25**:729 – 737
- [2] Peerlings, R. H. J., de Borst, R., Brekelmans, W. A. M. and de Vree, J. H. P., 1996. Gradient enhanced damage for quasi-brittle materials, *Int. J. for Num. Meth. in Eng.*, **39**:3391–3403.
- [3] Pijaudier-Cabot, G. and Bažant, Z., 1987. Nonlocal Damage Theory, *J. of Eng. Mech.*, **113**:1512–1533.
- [4] Bažant, Z. P. and Jirasek, M., 2002. Nonlocal integral formulations for plasticity and damage: survey of progress, *J. of Eng. Mech.*, **128**:1119–1149.
- [5] Pijaudier-Cabot, G., Krayani, A. and Dufour, F., 2009. Boundary effect on weight function in nonlocal damage model, *Eng. Frac. Mech.*, **76**:2217–2231.
- [6] Pijaudier-Cabot, G. and Dufour, F., 2010. Nonlocal damage model. Boundary and evolving boundary effects, *Eur. J. of Env. and Civil Eng.*, **14**:729–749.
- [7] Desmorat, R. and Gatuingt, F., 2010. Introduction of an internal time in nonlocal integral theories, In Bicanic et al (eds), *Computational Modelling of Concrete Structures; Proc. of Euro-C*, Mayerhofen, Austria.
- [8] Giry, C., Dufour, F. and Mazars, J., 2011. Modified nonlocal damage model based on stress state influence, *Int. J. of Solids and Struct.*, **48**:3431–3443.
- [9] Dufour, F., Pijaudier-Cabot, G., Choinska, M. and Huerta, A., 2008. Extraction of a crack opening from a continuous approach using regularized damage models, *Comp. & Conc.*, **5**:375–388.
- [10] Dufour, F., Legrain, G., Pijaudier-Cabot, G. and Huerta, A. 2012. Estimate of crack opening from a 2D continuum-based FE computation, *Int. J. for Num. and Anal. Meth. in Geomech.*, DOI:10.1002/nag.1097.
- [11] Tamayo-Mas, E. and Rodriguez-Ferran, A., 2012. From damage to discrete cracks:

the difficulties of transition. *11th Workshop on Numerical Methods in Applied Sciences and Engineering*. El Montany, Spain.

[12] Bottoni, M. and Dufour, F., 2010. Topo-

logical search of the crack path from a damage-type mechanical computation, In Bicanic et al (eds), *Computational Modelling of Concrete Structures; Proc. of Euro-C*, Mayerhofen, Austria; pp. 271-279.